Microdomain texture produced for an analog gray-scale technique using ferroelectric liquid crystals containing nanometer-scale particles

Eriko Matsui and Akio Yasuda
Sony Corporation Research Center, 174, Fujitsuka-cho, Hodogaya-ku, Yokohama-shi 240, Japan
(Received 2 August 1996; revised manuscript received 19 December 1996)

We have previously reported a novel gray-scale technique to be used with ferroelectric liquid-crystal (FLC) displays. The technique uses the microdomain texture, and the addition of nanometer-scale particles into the FLC mixture enables a wide distribution of threshold voltages within one pixel. We now report that threshold-voltage broadening is caused by an increase in the smectic-layer tilt angles and this microdomain growth is pinned by nanometer-scale particles. We found, moreover, that the microdomain texture can be classified into two types, depending on the switching process. [S1063-651X(97)12307-8]

PACS number(s): 42.70.Df, 64.70.Md

INTRODUCTION

A novel gray-scale technique to be used with ferroelectric liquid-crystal (FLC) displays has been previously reported. In the technique the addition of nanometer-scale particles into the FLC mixture enables a wide distribution of threshold voltages within one pixel element [1].

This time we report that one of the properties of this technique is the inhibited domain growth with switching. In a FLC without particles, domains grow even if voltage is not applied. However, in a FLC with particles, 1–10 μm domains appear when voltage is applied and do not grow under no electric field. Moreover, we show here two types of microdomain texture, which are caused by different increasing processes of their domains: In type A, the *number* of microdomains increases as applied pulse voltage is increased, and in type B, the *size* of microdomains increases as applied pulse voltage is increased. This domain growth scheme is clearly explained by Avrami theory.

Ferroelectric liquid crystal makes passive matrix addressing of displays of a large number of lines possible with memory effect. FLC displays have advantages such as a fast response time and wide viewing angle: however, gray-scale technology must be developed for the application to FLC's to video displays because of this bistable limitation. With the use of the addition of nanometer-scale particles into a novel FLC mixture (FLC1), video-rate display has been achieved.

EXPERIMENT

The properties of the ferroelectric liquid-crystal mixture (FLC1) used for these experiments are shown in Table I. The surface-modified nanometer-scale particles were amorphous titanium dioxide from Idemitsu Kosan Co., Ltd. Their average diameter was 17 nm. Nanometer-scale particles were added to FLC1 to the amount of 1 wt % and were dispersed homogeneously. The formation of SiO obliquely evaporated layers for alignment layers was made as previously reported [2]. The SiO alignment layers were assembled in an antiparallel configuration. The sample cells used for the electric-optic measurements consisted of two indium-tin-oxide-(ITO-) coated glass plates whose inside surfaces were coated with SiO film. The FLC mixture with nanometer-scale particles was injected into the space between the plates in the isotropic phase and gradually cooled down to room temperature. The diameter of the microdomain can be controlled by adjusting the cooling rate after the injection. The relationship between the diameter of the micro domain in type A and the cooling rate is shown in Fig. 1. The thickness of the LC layers was made 1.6 μm by SiO_2 spacers. To stabilize the microdomain structure, an electric-field treatment was applied to the cells at room temperature after the injection.

The gray scale was evaluated using the waveform shown

TABLE I. Properties of a novel ferroelectric liquid-crystal mixture (FLC1); video-rate display has been achieved.

Phase transition temperature (°C)	Iso 115 N* 105 SmA 69 SmC*
Melting point	−9 °C
Spontaneous polarization	10.1 nC cm^{-2}
Pulse width (under ±20 V/μm)	20.0 μs
(under ±12.5 V/μm)	32.0 μs
Contrast ratio (with 3:1 bias pulse)	>50

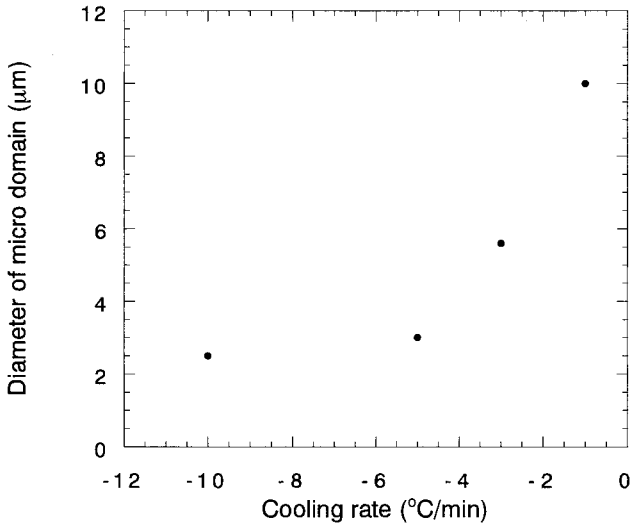

FIG. 1. Relationship between the cooling rate and diameter of microdomains in type A; the diameter of microdomains can be controlled by cooling the speed after injection.

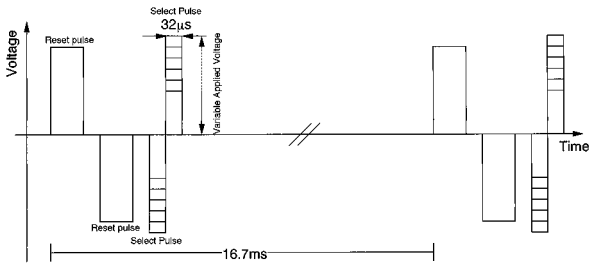

FIG. 2. Driving scheme for gray-scale evaluation. One frame is 16.7 ms for interlaced TV signals. The driving scheme applied consists of a bipolar reset and select pulses to ensure that there is no dc electric field which might degrade the liquid-crystal materials. The electrode potential is controlled by fixing the electrode ground level in order to apply the potential as the waveform. A reset pulse assures that the same starting situation (preferably the black state) is obtained before a gray level is written, which is necessary to obtain a reproducible gray level [3–5]. The gray level is determined by a bipolar select pulse with a variable amplitude.

in Fig. 2. One frame is 16.7 ms for interlaced TV signals. The driving scheme applied consists of bipolar reset and select pulses to ensure that there is no dc electric field which might degrade the liquid-crystal materials. The electrode potential is controlled by fixing the electrode ground level in order to apply the potential as the waveform. In an FLC cell, FLC molecules switch by an interaction between spontaneous polarizations and an applied electric field and are stable in the memory state. A reset pulse assures that the same starting situation (preferably the black state) is obtained before a gray level is written, which is necessary to obtain a reproducible gray level [3–5]. The gray level is determined by a bipolar select pulse with a variable amplitude. Electro-optical transmittance spectra in the memory state were measured using a photomultiplier between crossed polarizers. The transmittance dependence on the applied electric field was plotted for the *V-T* curves.

It is difficult for x rays to detect the layer tilt angle in each switching domain, because the switching domains are smaller than 10 μm in diameter and the measuring spot of x rays is 5 mm in diameter. In our work the apparent tilt angle of each switching domain at each applied voltage was optically monitored using a high-magnification objective lens combined with a condenser lens [6]. It was found that each microdomain showed bistability.

Two types of microdomain texture were prepared using

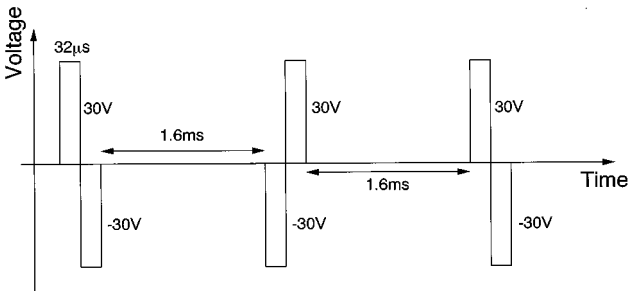

FIG. 3. Bipolar pulse waveform of electric-field treatment for the microdomain texture in type B; the *size* of microdomains increases as applied voltage is increased.

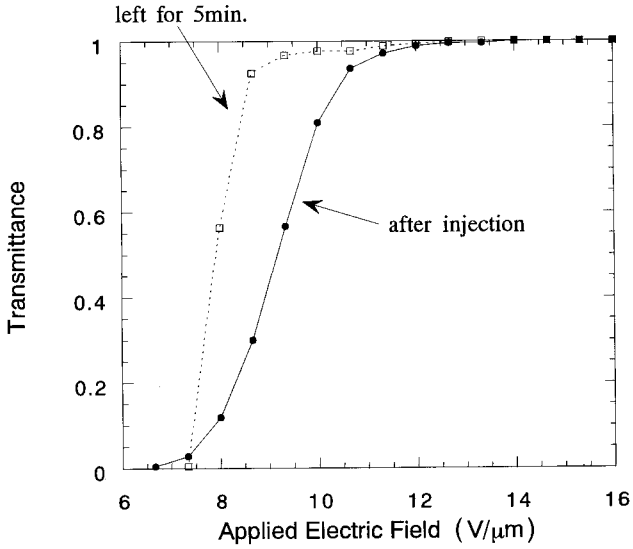

FIG. 4. *V-T* curves of a FLC panel at RT after injection and that of a FLC panel being left for 5 min in the isotropic phase. The *V-T* curves of the threshold voltage region of the cell of regular distribution particles before being left in isotropic phase were broadened. The *V-T* curves of the threshold voltage region of the cell of irregular distribution particles after being left in isotropic phase were steep.

two ways of electric-field treatment and cooling speed. For type A, preparation was very simple. After injection, the FLC was cooled $-5\,^{\circ}$C/min to room temperature and an electric field with a square waveform of 100 Hz under ± 20 V/μm was applied for 2 s. For type B, after injection, the FLC cell was cooled $-5\,^{\circ}$C/min to 67 °C (this temperature is 2 °C below the smectic-*A*–smectic-*C** phase transition temperature) and was cooled $-3\,^{\circ}$C/min to room temperature under an applied electric field with the bipolar pulse waveform shown in Fig. 3 in 14 min. Moreover, this cell was under an electric field with a square waveform of 100 Hz under ± 20 V/μm for 2 s at room temperature.

The photograph of the microdomain texture in the memory state at each applied voltage was taken between crossed polarizers using a microscopic camera system. This photograph of microdomain texture at each applied voltage allowed the determination of the ratio of area undergoing switching to the whole area an image processor.

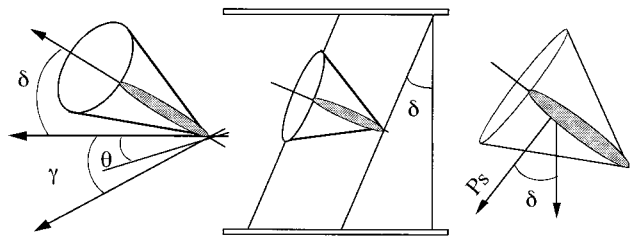

FIG. 5. Relation between the effective spontaneous polarization P_s and the apparent tilt angle γ with applied voltage with the SmC* tilt angle θ is defined. $\tan\gamma=\tan\theta/\cos\delta$ and $P_{s_{\rm eff}}=P_s\cos\delta$ show that the apparent tilt angle γ with applied voltage yields the layer tilt angle δ. And δ yields $P_{s_{\rm eff}}$; the P_s value is proportional to the threshold voltage, which we consider to be the origin of the $V_{\rm th}$ broadening phenomenon.

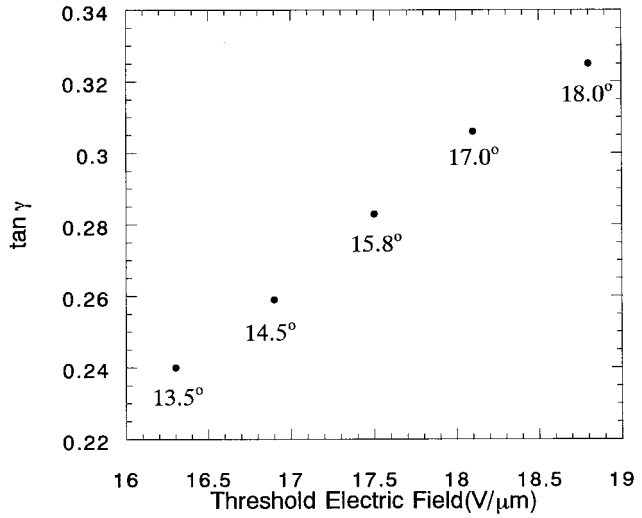

FIG. 6. Relationship between applied voltage and tanγ. It was found that each microdomain showed bistability. This result is coincident that larger apparent tilt angles correspond to larger layer tilt angles, which have a smaller effective P_s value for higher voltage required for switching.

INHIBITED GROWTH OF MICRODOMAINS AND MECHANISM OF MICRODOMAIN TEXTURE

The domain growth during switching in FLC's with conventional texture has been reported previously [7–9]. FLC switching with domain growth was observed with stroboscopic instruments. In a FLC with conventional texture, the domains nucleate and grow under electric field, and extend to the whole of the sample, growing and coalescing under no electric field. However, in a microdomain texture with a FLC with added nanometer-scale particles, the domains nucleate and grow under an electric field, and do not grow in the memory state under no electric field, giving the microdomain texture gray levels. The pinned growth of conventional domains brought about by the existence of fine dust in the FLC panel has been reported [10]. Similarly, we assumed that the microdomain growth is pinned by nanometer-scale particles. This assumption was proved to be correct by the following experiment.

Nanometer-scale particles, whose specific gravity is higher than that of FLC's by a factor of 3, easily sink in FLC materials during the isotropic phase. The V-T curves at room temperature (RT) of the FLC cell of microdomain texture with nanometer-scale particles and the same cell after being left for 5 min in the isotropic phase were plotted. The results are shown in Fig. 4. The threshold voltage region of the cell of regular distribution particles before being left in isotropic phase was broad. The threshold voltage region of the cell of irregular distribution particles after being left in isotropic phase was steep. Moreover, on the cell left 5 min in the isotropic phase, further growth of domains was observed by using a polarizing microscope. Regular distribution of particles in the layer is crucial for stable gray levels because the growth of domains can be pinned by the particles in the smectic layer.

The nanometer-scale particles are larger than FLC molecules by a factor of at least 5 even in an ideal case with no aggregation. These particles would influence alignment of FLC molecules. The broadening of the threshold region is brought about by an increase in the number of the smectic-layer tilt angles. The relation between the effective sponta-

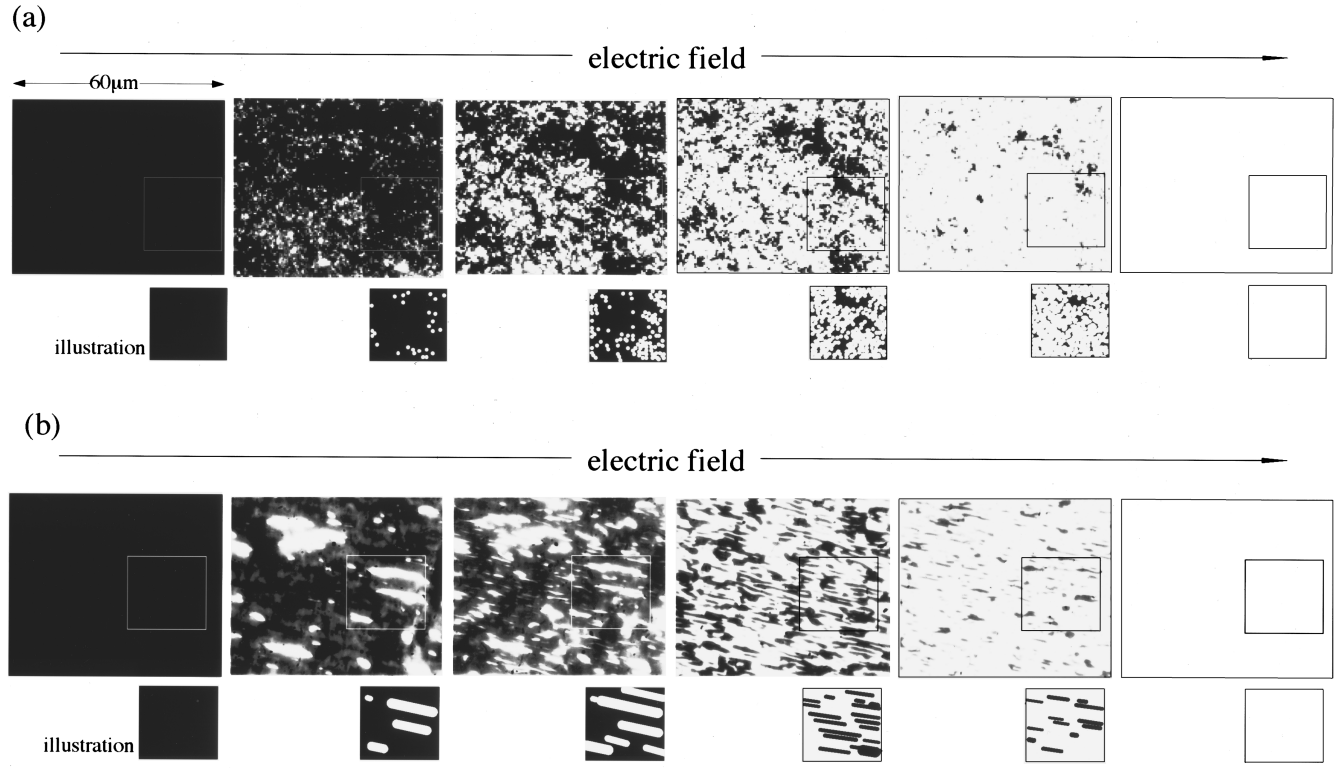

FIG. 7. Two types of increasing process of switching microdomains, photographs in size 60 μm$\times$50 μm and illustrations: (a) The *number* of microdomains increases with switching, and (b) the *size* of the microdomains increases with switching.

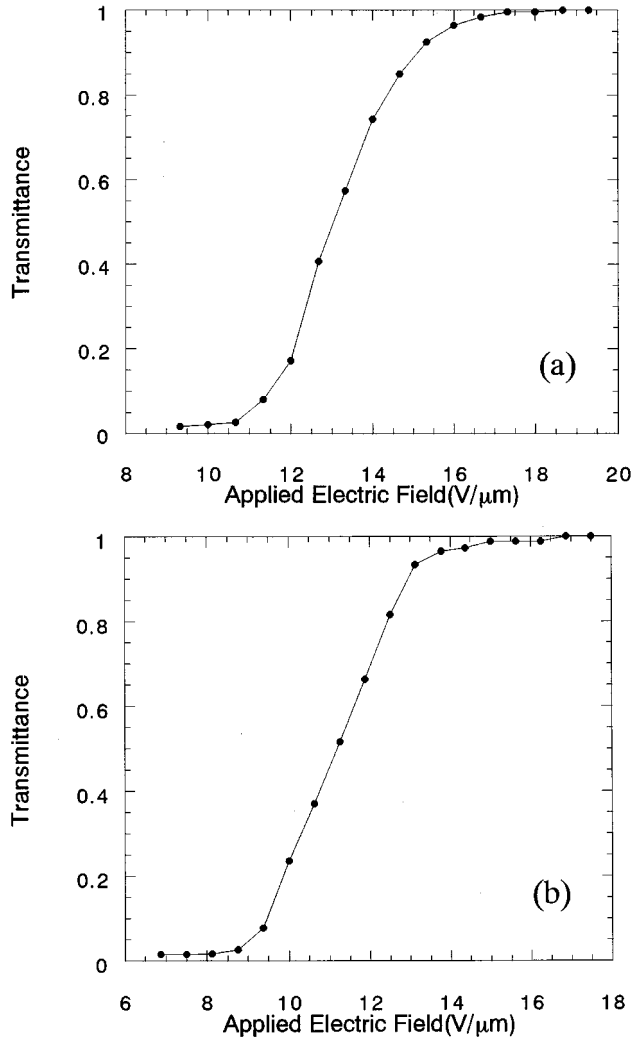

FIG. 8. *V-T* curves of the two types of texture: (a) The *number* of microdomains increases as applied voltage is increased, the shape is round, and (b) the *size* of the microdomains increases as applied voltage is increased; the curve has a more linear region.

neous polarization P_s and the apparent tilt angle γ with applied voltage with the SmC* tilt angle θ is defined in Fig. 5:

$$\tan\gamma = \tan\theta/\cos\delta, \tag{1}$$

$$P_{S_{\text{eff}}} = P_S \cos\delta. \tag{2}$$

Equations (1) and (2) show that the apparent tilt angle γ with applied voltage yields the layer tilt angle δ. And δ yields $P_{s\,\text{eff}}$; the P_s value is proportional to the threshold voltage, which we consider to be the origin of the V_{th} broadening phenomenon. Each microdomain shows bistability. The results of apparent tilt angle measurement are shown in Fig. 6. Larger apparent tilt angles correspond to larger layer tilt angles, which have a smaller effective P_s value. That is, higher voltage is required for switching. The linear relationship between applied voltage and $\tan\gamma$ is shown in Fig. 6. In the vicinity of nanometer-scale particles, FLC molecules are affected by the interaction between the molecules and the particle surface. This interaction produces deviations in the layer tilt and, thus, the V_{th} broadening phenomenon occurs.

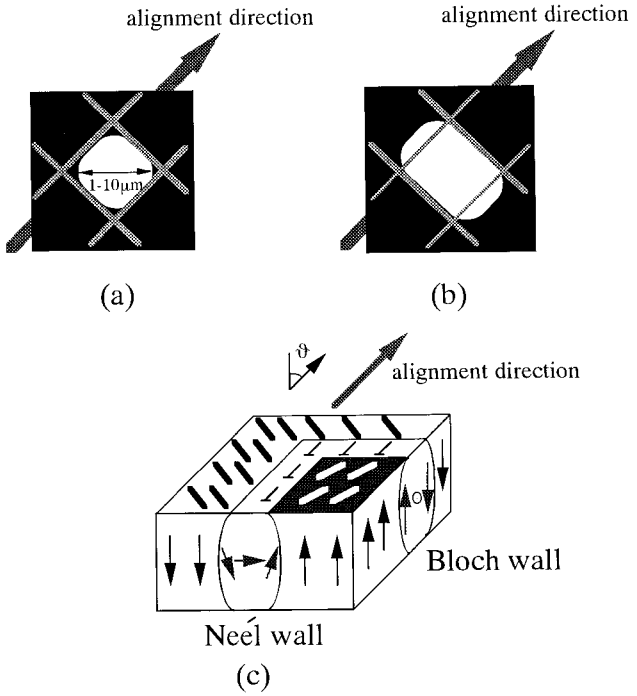

FIG. 9. In type-A microdomain texture, the domains are $1-5$ μm in size. Each domain is surrounded by layer-parallel and layer-normal walls. (b) In type B, domain growth occurs along the layer-parallel wall under applied pulse voltage increasing. (c) The FLC domain wall structure. The domains of FLC cells are separated by walls. Schematic of the surface-stabilized ferroelectric liquid-crystal structure, showing the tilted smectic with layers normal to the bounding plates, the director orientation *n* (short lines), and the accompanying ferroelectric polarization *P* (arrows). Pursuing the magnetic analogy further, the domain walls are ''Bloch-like'' if directed along the smectic layers and ''Neel-like'' if normal to the layers [10].

With the application of the above-mentioned electric field treatment, the structure of layers at various angles is stabilized, just as the chevron structure is uprighted with the application of an electric field [11]. Each microdomain shows bistability, does not grow further, and maintains a steep *V-T* curve at the threshold voltage. The microdomain texture has a large number of domains, for example, for 300 μm $\times 300$ μm 10^4 domains, each of which has different V_{th}, within as much area as one pixel. Thus the microdomain texture shows a broadening of the threshold region in one pixel element.

TWO TYPES OF MICRODOMAIN TEXTURE

Microdomain textures can be classified into two types depending on microdomain increasing processes as applied voltage is increased, by polarized microscopic observation. In type A, the *number* of the microdomains increases with switching, as in Fig. 7(a), while in type B, the *size* of the microdomains increases with switching, as Fig. 7(b). These two types of texture can be produced using same FLC1 and the surface-modified TiO_2 particle mixture by changing the alignment by temperature control and the application of an electric-field treatment after injection. Comparing the *V-T* curves, in type A the shape is round as in Fig. 8(a), while in type B the curve has more linear region as in Fig. 8(b). The

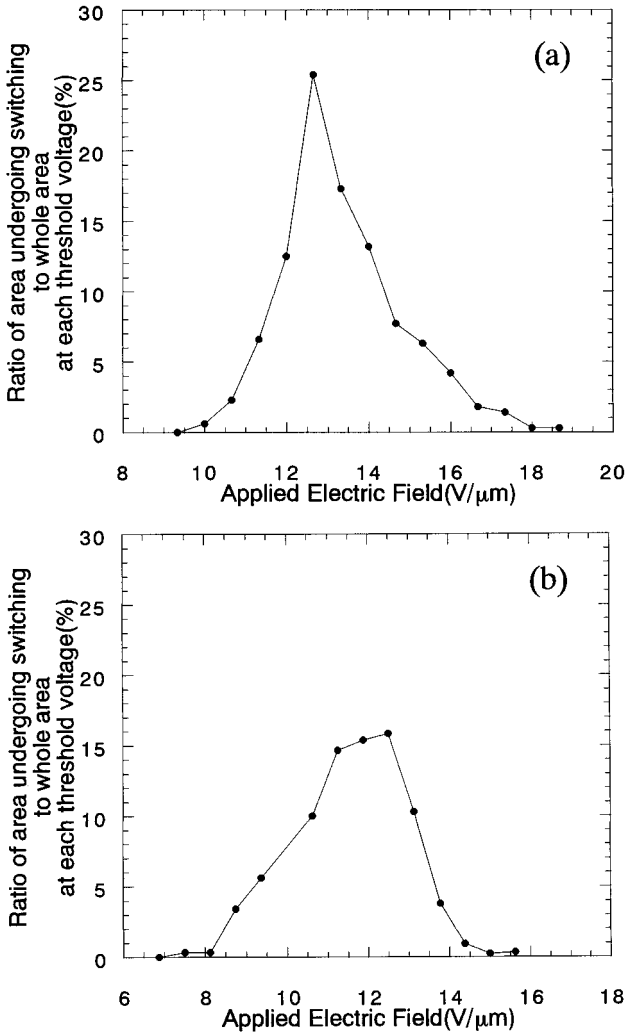

FIG. 10. Measurements of the ratio of the area undergoing switching to the whole area at each threshold voltage. On integration, the curve showing the ratio of the area undergoing switching to the whole area eventually produces the V-T curve from transmittance. (a) In the case of microdomain texture type A, tight pinning may be reflected by the sharp peak; that is, the domains are independent. (b) In the case of microdomain texture type B, domain growth occurs along the layer-parallel wall as applied pulse voltage is increased, as observed by a polarizing microscope. The domain growth was inhibited in the memory state. The loose pinning aids coalescence of the domains. Therefore, the microdomain textures can be classified into two types, depending on the strength of the domain wall.

easy controllability of the V-T curves is required for TV displays, because the controllability of the gray scale derived from the V-T curve shape is related to quality of display. It is indicated that the V-T curves can be controlled by texture control.

We now consider in more detail the FLC domain wall structure. The domains of the FLC cell are separated by walls, as shown in Fig. 9(c). This figure shows a schematic of the surface-stabilized ferroelectric liquid-crystal structure, showing the tilted smectic with layers normal to the bounding plates, the director orientation ν (short lines), and the accompanying ferroelectric polarization P (arrows). Pursuing the magnetic analogy further, the domain walls are ''Bloch-like'' if directed parallel to the smectic layers, and

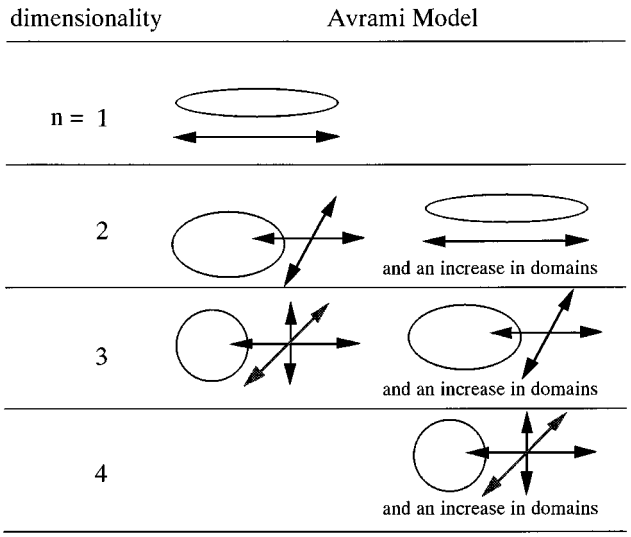

FIG. 11. Physical understanding of effective dimensionality ν of the Avrami model for microdomains [8,12–15]. For $n=1$, domain growth is one dimensional. For $n=2$, two-dimensional growth and one-dimensional growth plus an increase in the number of domains. For $n=3$, three-dimensional domain growth and two-dimensional growth plus an increase in the number of domains. For $n=4$, three-dimensional growth plus an increase in the number of domains.

''Néel-like'' if normal to the layers [10]. In type-A microdomain texture, the domains are 1–10 μm in size. Each domain is surrounded by layer-parallel and layer-normal walls, as observed by a polarizing microscope and illustrated in Fig. 9(a). The domain wall cannot suppress the growth of domains by itself, as described above. However, domains may have a tight pinning property because on the order of a hundred particles are calculated to exist in each domain. Figure 10(a) shows the measurement of the ratio of the area undergoing switching to the whole area at each threshold voltage. On integration, the curve showing the ratio of the area undergoing switching to the whole area eventually produces the V-T curve from transmittance. Tight pinning may be reflected by the sharp peak; that is, the domains are independent. On the other hand, in the case of microdomain texture type B, domain growth occurs along the layer-parallel wall as applied pulse voltage is increased, as observed using a polarizing microscope as shown in the illustration in Fig. 9(b). The domain growth was inhibited in the memory state and a broad peak is observed as in Fig. 10(b). Therefore, the loose pinning aids the coalescence of the domains. Thus microdomain textures can be classified into two types, depending on the strength of the domain wall.

DISCUSSION OF TWO TYPES OF MICRODOMAIN TEXTURE USING AVRAMI THEORY

Next, we explain the domain growth of the microdomain texture by applying the Avrami model. The Avrami model can be written as

$$t^{\nu} = -\ln[1 - S(t)/S(0)], \tag{3}$$

where ν is the dimensionality of the Avrami model, $S(t)$ is the reversed area at time t, and $S(0)$ is the total area. We regarded that $S(t)/S(0)$ is $T(t)$, where $T(t)$ is the transmit-

TABLE II. Dimensionality in the first (lower gradient) step; this result indicates that with the addition of the particles the surface anchoring may be weakened.

			Dimensionality intermediate-voltage region	Dimensionality high-voltage region
Microdomain texture:	type A	FLC with particles	0.4–0.8	1.0–2.5
Microdomain texture:	type B	FLC with particles	0–0.6	0–0.5
Conventional texture		FLC only	0	0

tance at time t. The physical understanding of the effective dimensionality ν of the Avrami model is summarized in Fig. 11 [8,12–15]. In the case of $n=1$, domain growth is one dimensional. In the case of $n=2$, there exist two possibilities, one is two-dimensional growth and the other is one-dimensional growth with an increase in the number of domains. In the case of $n=3$, again similar to the case of $n=2$, one possibility is three-dimensional domain growth and the other is two-dimensional growth plus an increase in the number of domains. For $n=4$, there is only three-dimensional growth plus an increase in the number of domains.

Using square-wave pulses in a variety of applied voltages, the relation between transmittance change and time was monitored for three type textures in type A with particles, in type B with particles, and in conventional texture without particles. We have classified the switching area into a high-voltage region, in which the switching area is the whole pixel element, and an intermediate-voltage region giving the microdomain texture for gray level as shown in Fig. 12. These switching areas (this transmittance) are calculated as in Ref. [15] and change logarithmically. The dimensionality ν is derived from the gradient of these plots. The scheme has been classified as a first (lower gradient) and second (higher gradient) step as in Fig. 12, depending on the dimensionality of the system, where $\ln\{-\ln[1-T(t)]\}$ is plotted against $\ln t$.

We summarize the results of the gradients of the curves in the three different systems, microdomain texture type A with particles, type B with particles, and conventional texture without particles. In the first step, dimensionality is shown in Table II. Dimensionality of types A and B with particles is 0–2. Dimensionality of conventional texture without particles is 0, and thus no switching occurs in this region. These results indicate that with the addition of the particles the surface anchoring may be weakened, and so switching is easier under lower voltages, while in the second step dimensionality shows the prominent feature of the microdomain texture in Table III. In the type-A cell, the dimensionality corresponds to $n=2$ or 3 or in between, that is, consistent with observation by a microscope in Fig. 7(a). In the type-B cell, the lower dimensionality reflects the smaller contribution of the increase in the number of domains, that is, consistent with observation by a microscope in Fig. 7(b). In the high-voltage region of the whole switching area, the existence of the particles clearly makes a difference. In type A with particles, with the two reinforced domain walls, the dimensionality in the high-voltage region is 3, the same as that in the intermediate region. In type B with particles, with the one reinforced domain wall, the dimensionality in the high-voltage region is higher than that in type A. In the conventional texture without particles, the dimensionality in the high-voltage region is the highest microdomain texture with particles. We considered that the particles pin the growth of domains and suppress the explosive domain growth indicated by a dimensionality over 4.

CONCLUSION

Threshold-voltage broadening was observed with the addition of nanometer-scale particles into a novel FLC mixture. An increase in the distribution of the smectic-layer tilt angles

TABLE III. Dimensionality in the second (higher gradient) step; in intermediate-voltage region with particles, the dimensionality is consistent with observation by a microscopy in Fig. 7. In the conventional texture without particles, the dimensionality in the high-voltage region is the highest microdomain texture with particles. We considered that the particles pin the growth of domains and suppress the explosive domain growth indicated by a dimensionality over 4.

			Dimensionality intermediate-voltage region	Dimensionality high-voltage region
Microdomain texture:	type A	FLC with particles	2.5–2.9	2.9–3.0
Microdomain texture:	type B	FLC with particles	1.7–2.4	2.6–3.7
Conventional texture		FLC only	3.1–3.3	3.4–5.5

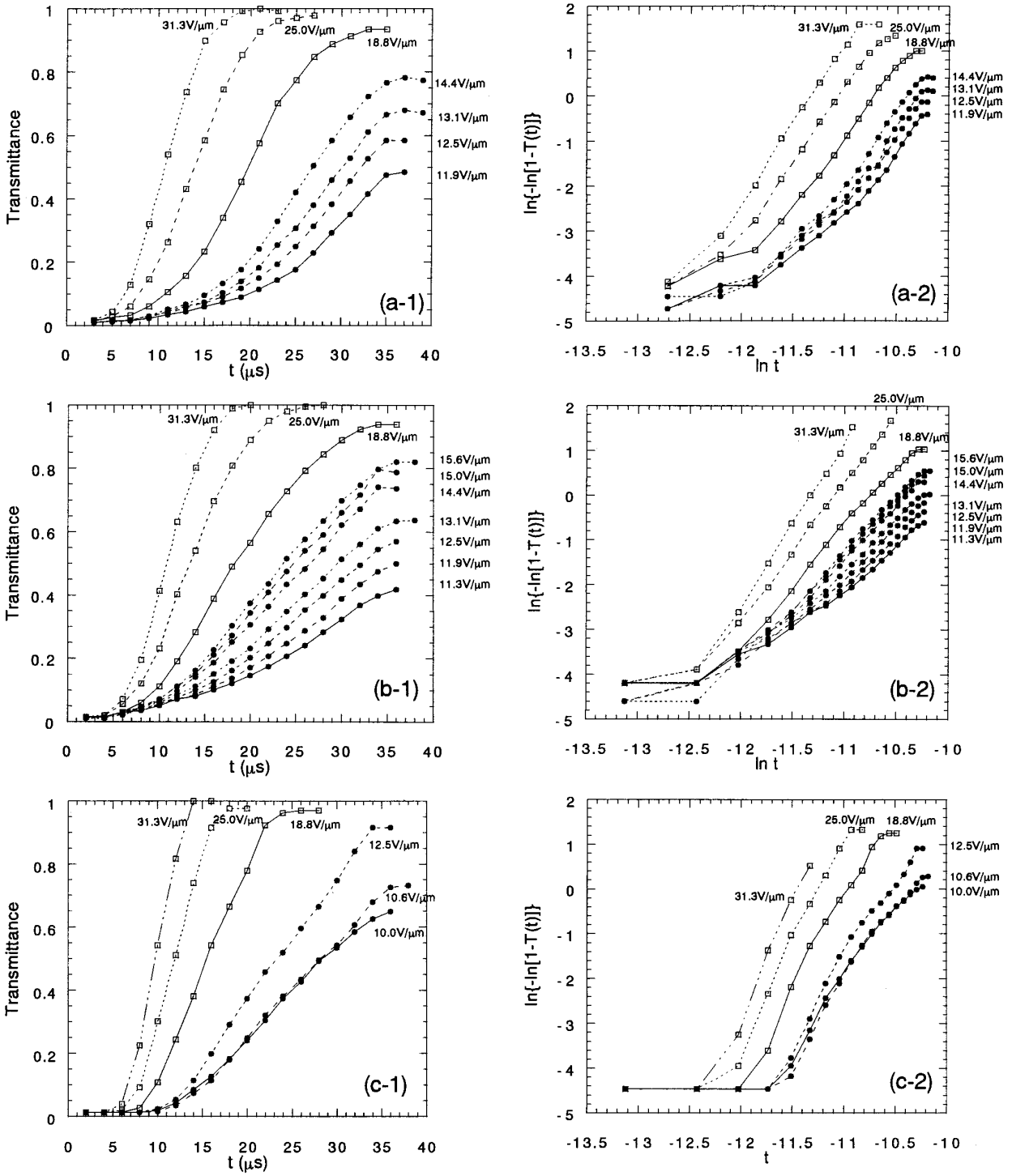

FIG. 12. Transmittance change versus time in three type textures (a-1) in type A with particles, (b-1) in type B with particles, and (c-1) in the conventional texture without particles using square-wave pulses in a variety of applied voltages. □, a high-voltage region, which switching area is the whole pixel element; ●, an intermediate-voltage region giving the microdomain texture for the gray level. These switching areas (this transmittance) as in Ref. [15] and change logarithmically. ln{−ln[1-$T(t)$]} is plotted against ln$t$, (a-2) in type A with particles, (b-2) in type B with particles, and (c-2) in the conventional texture without particles.

causes the V_{th} broadening. Two types of microdomain texture were found and classified into the domain number increasing type and the domain size increasing type. Various V-T curves can be obtained by controlling the texture with our FLC and particle mixtures.

ACKNOWLEDGMENT

The authors would like to express their sincere thanks to Professor Noel A. Clark of the University of Colorado for many useful discussions.

[1] A. Yasuda *et al.* Jpn., J. Appl. Phys. 1 **36**, 228 (1997).
[2] A. Yasuda *et al.*, in Proceedings of the 12th International Display Research Conference (Japan Display 92), 1992 (unpublished), p. 511.
[3] P. M. Maltese *et al.*, Ferroelectrics **85**, 265 (1988).
[4] W. Hartmann, J. Appl. Phys. **66**, 1132 (1989).
[5] W. Hartmann, Ferroelectrics **122**, 1 (1991).
[6] A. G. H. Verhulst and F. J. Stommels, Ferroelectrics **122**, 79 (1991).
[7] Y. Ishibashi and Y. Takagi, J. Phys. Soc. Jpn. **31**, 506 (1971).
[8] M. A. Handschy and N. A. Clark, Appl. Phys. Lett. **41**, 39 (1982).
[9] Y. Ouchi *et al.*, J. Appl. Phys. **26**, 1 (1987).
[10] N. A. Clark *et al.*, Mol. Cryst. Liq. Cryst. **94**, 213 (1983).
[11] H. Rieger *et al.*, SID 91 Digest **1991**, 396 (1991).
[12] M. Avrami, J. Chem. Phys. **7**, 1103 (1939).
[13] M. Avrami, J. Chem. Phys. **8**, 212 (1940).
[14] M. Avrami, J. Chem. Phys. **9**, 177 (1941).
[15] K. Dimmer *et al.*, J. Appl. Phys. **61**, 5467 (1987).